Pharm Res (2013) 30:751–760
DOI 10.1007/s11095-012-0917-z

RESEARCH PAPER

Interspecies Modeling and Prediction of Human Exenatide Pharmacokinetics

Ting Chen • Donald E. Mager • Leonid Kagan

Received: 5 July 2012 / Accepted: 15 October 2012 / Published online: 15 November 2012

ABSTRACT

Purpose To develop a model-based approach for interspecies scaling of the preclinical pharmacokinetics of exenatide and to predict concentration-time profiles in humans.

Methods A target-mediated drug disposition (TMDD) model was simultaneously fit to concentration-time profiles of exenatide over a wide range of intravenous (IV) and subcutaneous (SC) doses obtained from mice, rats, and monkeys. Allometric relationships were incorporated into the model to scale parameters based on species body weight. Human pharmacokinetic profiles following IV and SC administration were simulated using the final model structure and parameter estimates and compared to clinical data.

Results The final model provided a good simultaneous fit to all animal data and reasonable parameter estimates. Exenatide receptor binding affinity and baseline receptor concentrations were species-dependent. Absorption parameters from rat provided the best prediction of exenatide SC absorption in humans, but good predictions could also be obtained using allometric scaling of preclinical absorption parameters.

Conclusions A TMDD model combined with allometric scaling was successfully used to simultaneously describe preclinical data for exenatide from three animal species following both IV and SC administration. The majority of model parameters could be shared among the animal species and further used for projecting exenatide behavior in humans.

KEY WORDS allometric scaling · nonlinear absorption · nonlinear pharmacokinetics · target-mediated drug disposition · therapeutic proteins

T. Chen • D. E. Mager • L. Kagan (✉)
Department of Pharmaceutical Sciences, University at Buffalo
State University of New York
433 Kapoor Hall
Buffalo, New York 14260, USA
e-mail: lkagan@buffalo.edu

INTRODUCTION

Exendin-4 (exenatide) was originally isolated from the saliva of the Gila monster lizard (1). It is a 39-amino acid peptide, sharing 53% sequence homology with glucagon-like peptide-1 (GLP-1) (2). Unlike GLP-1, which is rapidly degraded by dipeptidyl pepdidase-4, exenatide is more stable and therefore exhibits a longer half-life and enhanced potency (3,4). The GLP-1 receptor is extensively distributed in various tissues like pancreas, brain, kidneys, and heart (5). Binding of exenatide to the GLP-1 receptor triggers multiple effects, including glucose-dependent stimulation of insulin secretion, glucose-dependent suppression of glucagon secretion, slowing of the gastric emptying, reduction of food intake and body weight, and protection of pancreatic beta cells (6,7).

The pharmacokinetics of exenatide has been studied in several species. In rats, the increase in C_{max} and AUC was not dose-proportional, suggesting that exenatide might exhibit nonlinear disposition (4). The Bateman function has been used to describe concentration-time profiles in rats following SC administration; however, a single set of first-order absorption and elimination rate constants was unable to account for the pharmacokinetic properties over all dose levels (8). A study in monkeys also showed that the clearance and elimination half-life change with dose (9). Target-mediated drug disposition (TMDD) models are frequently utilized to characterize nonlinear pharmacokinetics exhibited by therapeutic proteins and peptides (10,11). A TMDD model was applied to describe the pharmacokinetics of exenatide in a diabetic Goto-Kakizaki rat study. Exenatide elimination is assumed to occur through two pathways: either directly cleared from the circulatory system (e.g., renal catabolism) or internalized and degraded in the form of drug-receptor complex throughout the body. Due to the limited capacity of the receptor-mediated elimination,

high drug concentration (as compared to receptor concentration) resulted in saturation of this pathway and nonlinear pharmacokinetics (12).

Allometric scaling is frequently used for predicting pharmacokinetic parameters in humans from laboratory animal data. This is based on the assumption that there are anatomical, physiological and biochemical similarities among animals, which can be expressed mathematically by the power function (13):

$$P = a \cdot BW^b \quad (1)$$

where P is a parameter of interest, BW is the species body weight, and a and b are the coefficient and the exponent of the allometric equation. The typical values of exponents for the clearance, the volume of distribution, and the elimination rate constant are 0.75, 1, and −0.25; however, a wide range of values for these two parameters have been reported (14,15). Although allometric scaling is extensively used to predict pharmacokinetic parameters for small molecules, the examples for macromolecules are relatively scarce. More importantly, nonlinear behavior that is frequently observed for macromolecules, renders traditional interspecies scaling of apparent volumes and clearances unsuitable for predicting the dose-dependent pharmacokinetics in human.

The goal of this work was to develop a model-based approach for interspecies scaling of the pharmacokinetics of exenatide following IV and SC administration based preclinical data and to further evaluate this approach for predicting the concentration-time profiles of exenatide in humans. In clinical practice, many therapeutic proteins are administered by SC injection rather than by the IV route. Although several animal species are usually evaluated during preclinical drug development, predicting the SC absorption behavior and the bioavailability in humans remains a very complex task (16).

METHODS

Data Source

This secondary data analysis was exempt from IACUC and informed consent. Mean concentration-time profiles of exenatide following different modes of administrations to rat and monkey studies were captured by computer digitization from the literature (4,17). Partial pharmacokinetic data in mice and exenatide profiles in humans were provided by Amylin Pharmaceuticals, Inc from published studies, and all studies are summarized in Table I. The concentration values of exenatide were converted to pM units and doses were converted to pmole/kg using the drug molecular weight (4,187 g/mol).

Data Analysis

A non-compartmental analysis of animal IV concentration-time profiles was performed for initial data evaluation. Area under the concentration-time curve from time zero to infinity (AUC), volume of distribution at steady state (V_{ss}) and clearance (CL) were calculated. In addition, a standard linear two-compartment model was used to fit each IV dataset separately. The volume of the central compartment (V_c), first-order distribution rate constants to and from the peripheral compartment (k_{pt} and k_{tp}) and the elimination rate constant (k_{el}) were estimated. The analysis was performed using Phoenix (Pharsight, Mountain view, CA). Parameters were plotted as a function of the mean body weights of different species to evaluate potential relationships.

For simultaneous modeling, the nonlinear disposition of exenatide was assumed to result from high affinity binding and limited capacity of the GLP-1 receptor. Hence, a TMDD model was used to mechanistically represent the interaction of the drug and receptor at the molecular level, and the final model is shown in Fig. 1 (18). Free exenatide (C) in the central compartment binds to free receptor (R) to form the drug-receptor complex (RC). The second-order rate constant k_{on} and first-order rate constant k_{off} are used for the association and dissociation processes. Free exenatide can also distribute to and from a peripheral compartment (A_T) with first-order rate constants, k_{pt} and k_{tp}. The main elimination route for exenatide is glomerular filtration (19); however, in nephrectomized rats, exenatide was still eliminated at 0.86 mL/min compared to 4.3 mL/min in rats who underwent sham surgery (4). This suggests alternate elimination pathways, such as target-mediated endocytosis. Therefore, two elimination pathways were incorporated into the model: free drug can be eliminated directly from the central compartment with the first-order rate constant k_{el}, and RC can be internalized and degraded (k_{int}) by receptor-mediated endocytosis. Turnover of GLP-1 receptor has been identified in an *in vitro* study (20); hence, the receptor turnover rate constants k_{syn} and k_{deg} were included in the final model. Zero-order production rate (k_{syn}) is a secondary parameter, equal to the product of k_{deg} and $R_{tot}(0)$ (the concentration of receptor at baseline). The absorption kinetics of exenatide after SC injection could not be adequately described using a single first-order rate constant. Therefore, drug absorption in the final model was characterized by the Michaelis-Menten function, where V_{max} represents the maximum absorption rate and K_m is the substrate amount of exenatide in absorption site (SC) when

the reaction rate is half of V_{max}. The model can be described by the following equations:

$$\frac{dSC}{dt} = -\frac{V_{max} \cdot SC}{K_m + SC} \qquad SC(0) = \text{Dose or } 0 \text{ (IV)} \qquad (2)$$

$$\frac{dC}{dt} = \frac{V_{max} \cdot SC}{Vc \cdot (K_m + SC)} - (k_{el} + k_{pt}) \cdot C + k_{tp} \cdot \frac{A_T}{V_c} - k_{on} \cdot R \cdot C + k_{off} \cdot RC \qquad C(0) = \frac{Dose}{V_c} \text{(IV) or } 0 \text{ (SC)} \qquad (3)$$

$$\frac{dA_T}{dt} = k_{pt} \cdot C \cdot V_c - k_{tp} \cdot A_T \qquad A_T(0) = 0 \qquad (4)$$

$$\frac{dR}{dt} = k_{syn} - k_{on} \cdot R \cdot C - k_{off} \cdot RC - k_{deg} \cdot R \qquad R(0) = R^0_{tot} \qquad (5)$$

$$\frac{dRC}{dt} = k_{on} \cdot R \cdot C - (k_{off} + k_{int}) \cdot RC \qquad RC(0) = 0 \qquad (6)$$

V_c and k_{el} were scaled with body weight according to the power equation (Eq. 1). The allometric function was incorporated into the TMDD model and pharmacokinetic data for mouse, rat and monkey following both administration routes and all dose levels were co-modeled and fitted simultaneously.

Concentration-time profiles following IV and SC administration in humans were simulated and the results were compared to the available clinical data. V_c and k_{el} for humans were scaled using Eq. 1 according to the body weights from the corresponding studies (Table I), in which allometric exponents were fixed to 1 and −0.25. Assuming that monkey and human have the most physiological similarity, the monkey values for k_{off} and R^0_{tot} were used for simulating human exenatide pharmacokinetics. All other parameters related to systemic distribution and elimination were shared between animal and human models. Two approaches were explored for predicting the absorption of exenatide in humans after SC administration. The first method was based on the assumption that the absorption

Table I Sources of Exenatide Pharmacokinetic Data

Species	n	Mean body weight (kg)	Administration route	Dose (pmol/kg)	Assay	Reference
Mouse (CD-1)	5–6	0.03[a]	IV	5.97×10^4	ELISA	(40)
	4	0.03	IV	4.78×10^3	ELISA	Amylin Pharmaceuticals Inc.
	4	0.03	SC	8.60×10^2		
				4.78×10^3		
				4.78×10^4		
Rat (SD)	4–7	0.36	IV	1.39×10^3	ELISA	(4)
				1.39×10^4		
				1.39×10^5		
	4–6	0.4	IV infusion (180 min)	4.17×10^3		
				4.17×10^4		
				4.17×10^5		
	4–7	0.36	SC	1.39×10^3		
				1.39×10^4		
				1.39×10^5		
Monkey (Rhesus)	9	4.3	IV	7.17×10^2	Radioimmunoassay	(9)
			SC	2.39×10^2		
				7.17×10^2		
				2.39×10^3		
Human	11	79.5	IV infusion (360 min)	2.38×10^1	Immunoenzymetric assay	(38) [b]
	8	88	SC	2.39×10^1		(39) [b]
				4.78×10^1		
				7.17×10^1		
				9.55×10^1		
	8	129	SC	4.78×10^0		
				1.19×10^1		
				2.39×10^1		

[a] Value is not reported in the original publication; a common value for the species was assigned

[b] Mean data were available from publication, individual data were provided by Amylin Pharmaceuticals Inc

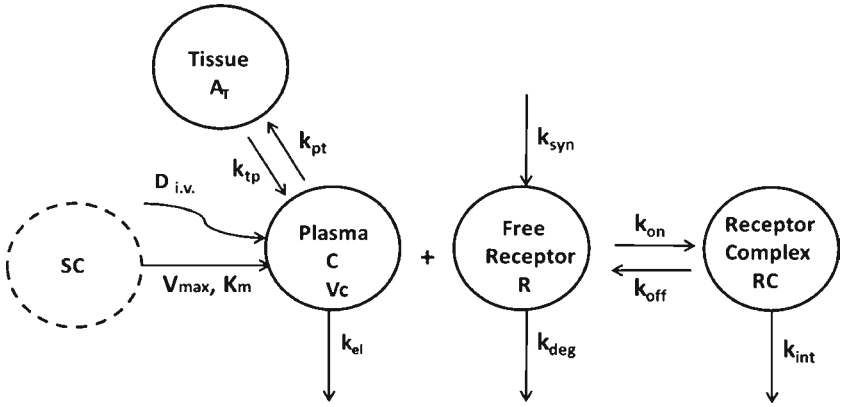

Fig. 1 Model scheme used to characterize exenatide pharmacokinetics in mice, rats, monkeys, and humans.

kinetics in humans was similar to one of the animal species, and hence three separate sets of V_{max} and K_m values (as estimated at the previous stage) were used to simulate human pharmacokinetics. The second method assumed that human V_{max} and K_m could be predicted by scaling values from preclinical species using the allometric approach (Eq. 1).

All model fitting and simulations were conducted using MATLAB R2009a (The MathWorks, Natick, MA) with the maximum likelihood method. The variance model was $V_i = (\sigma \cdot Y)^2$, with V_i as the variance of the i^{th} data point, σ is the variance model parameter, and $Y(\theta, t_i)$ is the i^{th} predicted value from the pharmacokinetic model. The final model was selected according to system convergence, Akaike Information Criterion, estimator criterion value for the maximum likelihood method, and visual inspection of the fitted curves.

RESULTS

Table II summarizes the preclinical pharmacokinetic parameters for IV exenatide obtained by non-compartmental analysis and two-compartment model fitting. For the rat, CL and V_{ss} decreased with increasing dose level, which is a common phenomenon for drugs following TMDD behavior. Accordingly, fitting the two-compartment model to the data resulted in relatively poor fits with low precision of the estimated parameters (data not shown). For mice and monkeys, the available data for IV administration was limited and dose-dependency of the volume of distribution and clearance was not observed (Table II). The values for CL and V_{ss} obtained by non-compartmental analysis were highly correlated with body weight (Fig. 2).

Mean plasma concentration-time profiles of exenatide following IV and SC administration to mice, rats, and monkeys are shown in Fig. 3. In general, the proposed pharmacokinetic model allowed for a good simultaneous description of all animal data and model parameters were estimated with reasonable precision (Table III). Some systematic deviations were obtained for the low IV dose in mice and monkeys, which could result from the limited number of observations and dose levels in these data sets (and therefore their low impact on parameter estimation). The allometric exponents for V_c and k_{el} were initially allowed to be estimated. The estimates were similar to theoretical values and were eventually fixed to 1 and −0.25. Scaling k_{pt} and k_{tp} with body weight did not improve modeling fitting, thus these parameters were shared among the three species. Interestingly, this identical interspecies scaling approach was successfully applied for modeling interferon pharmacokinetics in several animal species and humans (21). In the final model, the same k_{on} was used for all species; however, k_{off} and R^0_{tot} were species-dependent assuming different receptor densities and binding affinities. To improve the precision of parameter estimation, R^0_{tot} terms were fixed during the final run to previously estimated values. The baseline receptor density in rats was similar to a previously reported value (12). Other parameters related to the receptor were shared among species.

Although the exact mechanism of exenatide absorption is unknown, a Michaelis-Menten type function was successfully applied to describe the absorption phase for clinical data (22). Species-specific parameters (V_{max} and K_m) were required to successfully capture the absorption behavior of exenatide. Initially, a first-order rate constant for drug degradation at the absorption site was incorporated; however, the estimated value was close to zero, and therefore, this term was excluded from the final model.

The ability to predict exenatide pharmacokinetics in humans was evaluated by simulation. Figure 4 shows simulation results overlaid with the pooled observed plasma exenatide concentrations following IV and SC administration to humans. The concentration-time profile of exenatide after IV infusion in humans was successfully predicted using all shared and species-specific parameters (R^0_{tot} and k_{off}) for monkey (Fig. 4, Study A). The first method for predicting SC absorption kinetics in humans was to evaluate whether the combination of V_{max} and K_m from one of the preclinical species could be directly applied for human data. Interestingly, utilization of absorption parameters from monkey did not predict

Table II Preclinical Pharmacokinetic Parameters of Intravenous Exenatide Calculated by Non-compartmental Analysis and Two-Compartmental Modeling

Species	Dose pmol/kg	Route	Non-compartmental analysis			Two-compartmental model				
			AUC min·pM	CL L/min	V_{ss} L	V_c L	k_{pt} min^{-1}	k_{tp} min^{-1}	k_{el} min^{-1}	CL_D L/min
Mouse	4.78×10^3	IV	4.78×10^5	3.00×10^{-4}	3.59×10^{-3}	3.86×10^{-3}	2.68×10^{-3}	4.67×10^{-2}	8.05×10^{-2}	1.04×10^{-5}
	5.97×10^4		5.82×10^6	3.08×10^{-4}	8.56×10^{-3}	NC	NC	NC	NC	NC
Rat	1.39×10^3	IV	5.35×10^4	9.34×10^{-3}	1.32×10^{-1}	4.86×10^{-2}	9.30×10^{-2}	6.48×10^{-2}	1.82×10^{-1}	4.20×10^{-3}
	1.39×10^4		1.22×10^6	4.09×10^{-3}	8.11×10^{-2}	5.83×10^{-2}	1.67×10^{-2}	3.03×10^{-2}	7.49×10^{-2}	2.32×10^{-3}
	1.39×10^5		1.40×10^7	3.57×10^{-3}	7.69×10^{-2}	5.30×10^{-2}	2.03×10^{-2}	2.36×10^{-2}	7.73×10^{-2}	1.94×10^{-3}
Rat	4.17×10^3	IV infusion	1.48×10^5	1.10×10^{-2}	2.34×10^{-1}	9.71×10^{-2}	2.56×10^{-2}	3.31×10^{-2}	1.05×10^{-1}	2.48×10^{-3}
	4.17×10^4		3.03×10^6	4.94×10^{-3}	1.02×10^{-1}	5.73×10^{-2}	1.99×10^{-2}	2.69×10^{-2}	8.82×10^{-2}	1.14×10^{-3}
	4.17×10^5		4.50×10^7	3.34×10^{-4}	5.48×10^{-3}	5.45×10^{-3}	1.33×10^{-1}	3.20×10^{-2}	4.45×10^{-1}	7.25×10^{-4}
Monkey	7.17×10^2	IV	2.27×10^5	1.36×10^{-2}	3.91×10^{-1}	6.80×10^{-2}	9.39×10^{-3}	3.43×10^{-2}	4.83×10^{-2}	2.75×10^{-3}

NC not calculated; pharmacokinetic profile had an insufficient data. *AUC* area under the concentration-time curve; *CL* clearance; V_{ss} steady-state volume of distribution; V_c volume of the central compartment; k_{pt} and k_{tp} distribution rate constants; k_{el} elimination rate constant; CL_D, distribution clearance

human SC profiles well. The simulated absorption rate was overpredicted, resulting in a shorter T_{max} and faster elimination as compared to the observed human data (Fig. 4, dashed lines). Simulations with mouse absorption parameters also performed poorly (data not shown). In contrast, the combination of rat V_{max} and K_m provides a good prediction of the exenatide pharmacokinetics following SC administration in humans (Fig. 4, solid lines).

The correlation between V_{max} and K_m with body weight was evaluated as an alternative approach for predicting human absorption. V_{max} is highly correlated with body weight with r^2=0.996 (Fig. 5, left panel). Although K_m appears less correlated with body weight, the coefficients and exponents obtained from both regressions were used to calculate corresponding parameters for humans. Interestingly, the resulting simulation profiles for human SC studies overlapped with the simulated lines that were obtained using the first method and rat V_{max} and K_m values (results not shown).

DISCUSSION

Dose-dependent pharmacokinetics exhibited by exenatide (12) is a characteristic feature frequently observed for peptide and protein drugs due to the interaction with high-affinity and low-capacity receptor systems in the body. Conventional allometric approaches might not be appropriate for predicting human disposition, as they do not account for dose-dependency of pharmacokinetic parameters. Furthermore, these methods are traditionally focused on clearance and volume terms, and the scalability of the absorption kinetics has not been fully investigated. The search for covariates that can be used to explain inter-subject variability is common practice in the analysis of clinical pharmacokinetic data. Clearance and volume terms frequently contain allometric expressions that define individual parameters based on subject body weight. Examples of interspecies scaling based on allometric expressions incorporated into structural pharmacokinetic models are still rare. Two-compartment models for sumatriptan and oxytetracycline have been reported, where IV data were fitted across multiple species and the allometric coefficients and exponents for pharmacokinetic parameters were estimated simultaneously (23,24). A similar approach was applied to a more complex TMDD system, in which the pharmacokinetics of type I interferons (that bind to IFNAR receptor system) were characterized in mice, rats, monkeys, and humans following IV administration (21). In contrast to exenatide, analogs of human interferons are inactive in rodents (which is attributed to a lack of receptor binding in these species); therefore, the scalability of receptor-related parameters over a whole range of body weights could not be assessed.

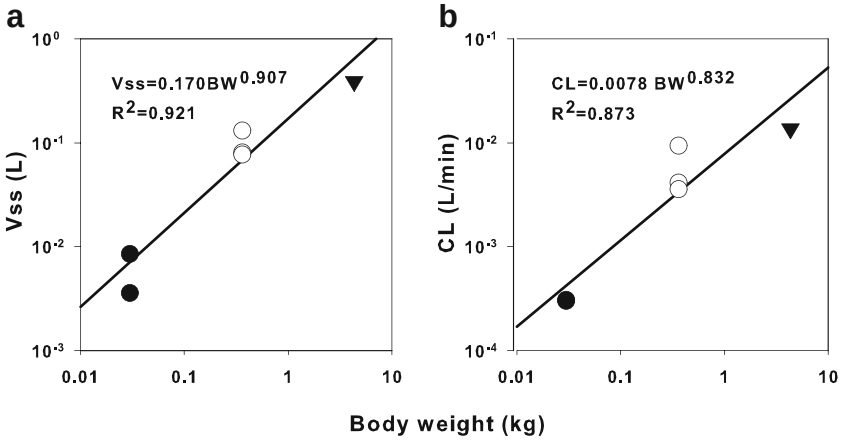

Fig. 2 Allometric scaling of volumes and clearances for IV doses of exenatide administered to mice, rats and monkeys. (**a**) Volume of distribution at steady state (Vss) and (**b**) clearance (CL) calculated by non-compartmental analysis. *Symbols* represent values from different species (mouse—●; rat—○; monkey—▼). *Lines* represent regression lines (Eq. 1).

The allometric exponents for V_{ss} and CL (Fig. 1), obtained by non-compartmental analysis, were within the ranges previously reported for other therapeutic proteins (0.65–0.84 for CL and 0.84–1.02 for V_{ss}) (25). Owing to dose-dependent pharmacokinetics, traditional allometry could not be used for predicting exenatide behavior in humans. In a recently published analysis, Gao and Jusko applied a TMDD model to describe exenatide pharmacokinetics separately in rats, monkeys, and humans. Subsequently, correlations between the estimated parameters and species body weights were assessed using regression analysis (26). However, due to a limited IV doses in humans and monkeys, some of the parameters could not be

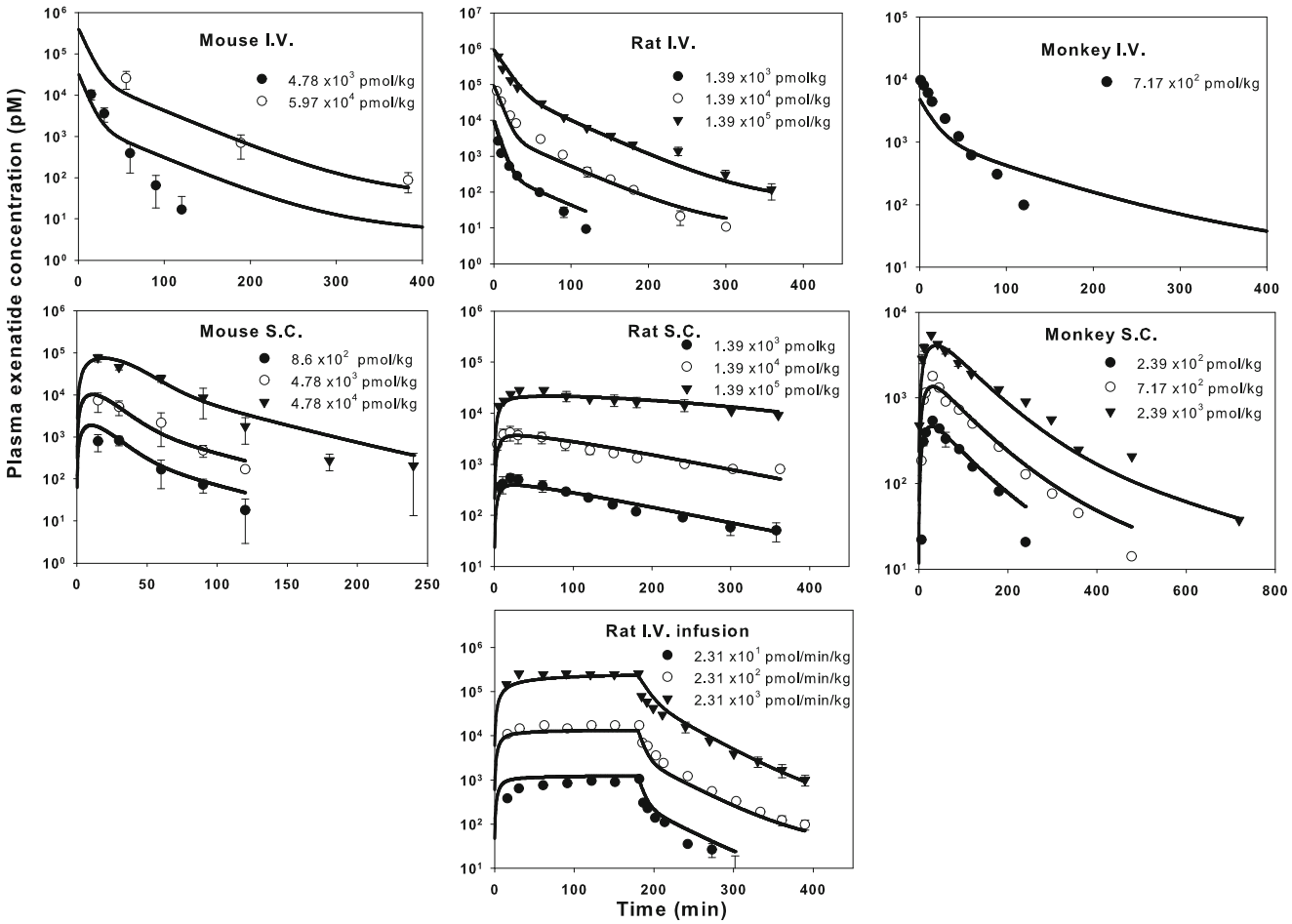

Fig. 3 Time-course of exenatide concentration in mice, rats, and monkeys. *Symbols* represent mean concentration (±SD) data, and *solid lines* are model-fitted profiles after simultaneous fitting of exenatide data for all species.

Table III Final Pharmacokinetic Model-Estimated Parameters

Parameter (units)	Description	Estimate (CV%)
V_c (L·kg^{-1}) [a]	Central volume of distribution	1.4×10^{-1} (7)
k_{el} (min^{-1}· kg^{-1}) [a]	Elimination rate constant for free exenatide	3.2×10^{-2} (8)
k_{pt} (min^{-1})	Distribution rate constant	2.6×10^{-2} (15)
k_{tp} (min^{-1})	Distribution rate constant	2.7×10^{-2} (8)
k_{deg} (min^{-1})	Degradation rate constant for free receptor	1.55×10^{0} (18)
k_{int} (min^{-1})	Rate constant of internalization for exendine-4-receptor complex	2.3×10^{-3} (41)
k_{on} (pM^{-1}·min^{-1})	Second-order association rate constant	1.7×10^{-5} (8)
K_{off}_mouse (min^{-1})	First-order dissociation rate constant	2.3×10^{-4} (52)
K_{off}_rat (min^{-1})		5.2×10^{-5} (46)
K_{off}_monkey (min^{-1})		1.5×10^{-3} (58)
R^0_{tot}_mouse (pM)	Receptor concentration at baseline	1.0×10^{3} (N/A)[b]
R^0_{tot}_rat (pM)		5.2×10^{3} (N/A)[b]
R^0_{tot}_monkey (pM)		5.2×10^{2} (N/A)[b]
V_{max}_mouse (pmol·min^{-1})	Maximum absorption rate	8.3×10^{1} (45)
V_{max}_rat (pmol·min^{-1})		2.4×10^{2} (19)
V_{max}_monkey (pmol·min^{-1})		5.8×10^{2} (62)
K_m_mouse (pmol)	Amount of exenatide when absorption rate is half maximal	9.1×10^{2} (61)
K_m_rat (pmol)		3.4×10^{4} (24)
K_m_monkey (pmol)		1.8×10^{4} (74)

[a]Value represents an allometric coefficient scaled to body weight

[b]Not applicable; fixed value

estimated with sufficient precision. In contrast, this study includes data from more animal species (mice, rats, and monkeys), and the mechanistic TMDD model was used to co-model data from all animal species. Allometric relationships for V_c and k_{el} were incorporated into the final model structure, and human clinical data were not utilized for model development but rather to only qualify the model predictive performance.

The quasi-equilibrium approximation of the TMDD model failed to provide a reasonable fit of all preclinical exenatide profiles (data not shown) (27). The full TMDD model provided more flexibility, good simultaneous fits, and satisfactory precision of parameter estimates (Fig. 3 and Table III). In addition, species-specific receptor density and binding affinity were required for capturing the data. During initial model runs, both k_{on} and k_{off} were allowed to be species-specific; however, the estimates for k_{on} for different species were similar. Therefore, a single shared k_{on} and separate k_{off} values were estimated. The estimated value of k_{on} is 4 times lower than an *in vitro* measurement (20), which might be attributed to differences between *in vivo* and *in vitro* conditions.

A wide range of exenatide receptor binding affinities ($K_D = k_{off}/k_{on}$) is available in the literature. Reported values for K_D in humans are usually higher than those for rat (28–31), and are consistent with this study (Table III). Experimentally measured affinities in mice and monkeys could not be found in the literature.

The final model included separate R_{tot} values for each animal species. Species differences in GLP-1 receptor expression were reported between humans and rodents in an *in vitro* study (5). In lung and thyroid tissues, rat exhibited the highest GLP-1 receptor density, followed by mouse and human tissues. Assuming that these tissues are representative for the whole body, the rank order is consistent with our modeling results. In addition, the baseline R_{tot} for rat estimated in this study is similar to a prior estimate (26).

For drugs administered by extravascular routes, in addition to scaling distribution and elimination processes, approaches for prediction of absorption kinetics and bioavailability are required for successful translation of preclinical findings to humans. The systemic uptake of macromolecules following SC administration is dependent on a complex interplay of various processes at the absorption site. Multiple factors, including anatomical site of injection and dose level, can influence the rate and the extent of absorption (10,32,33). Interspecies variability in SC absorption due to species-dependent factors (e.g., skin morphology) can be substantial, and the best animal model(s) for predicting SC absorption in humans remains to be identified (16).

Although methods for predicting oral absorption of small molecules are promising (34–36), scaling absorption kinetics for extravascular routes is limited. For SC administered pegylated erythropoietin, k_a was scaled with body weight among four species and the allometric exponent was estimated to be −0.147 (37). For cases in which absorption kinetics varies with dose, separate values for the absorption rate constant or bioavailability are frequently utilized for each dose level (10,20,26). Whereas this approach might be

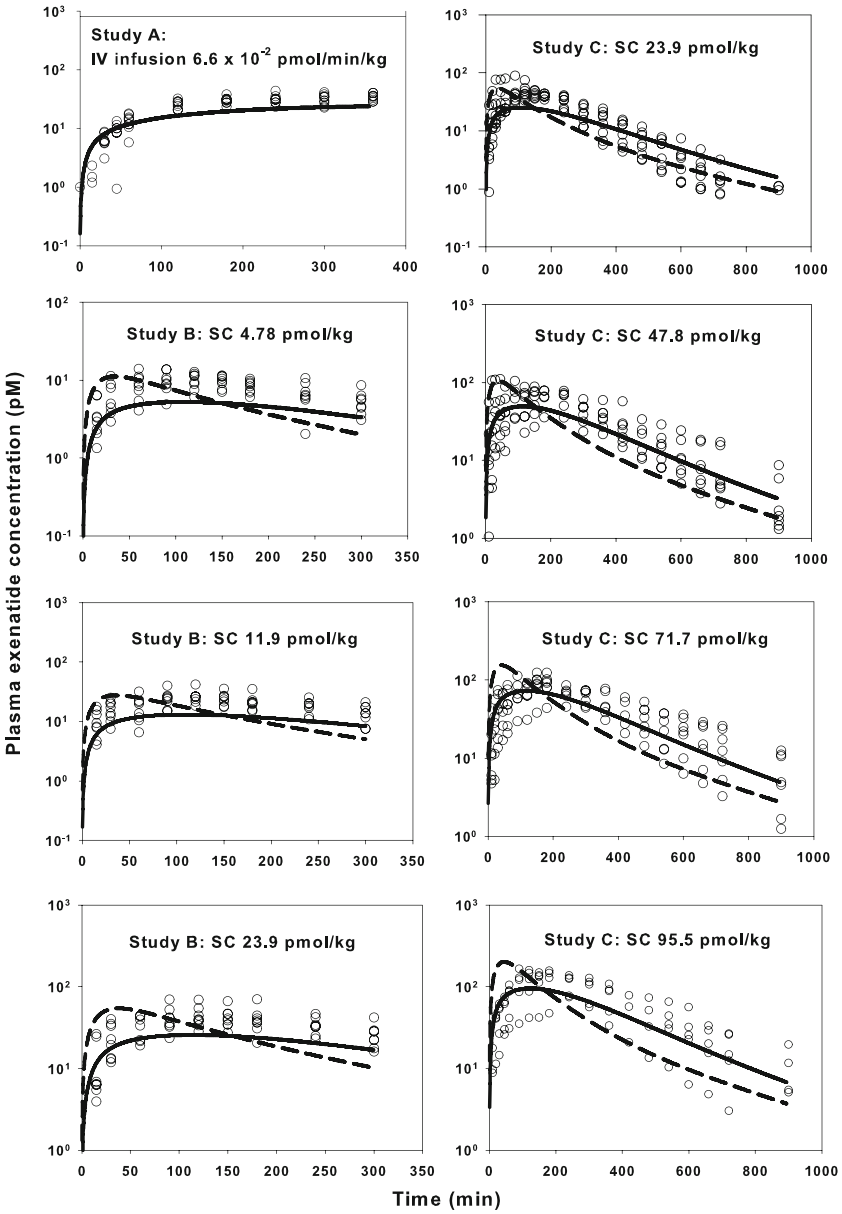

Fig. 4 Time-course of exenatide concentrations following IV infusion and SC administration in humans. *Symbols* are observed clinical data and model-simulated profiles are shown using rat (*solid lines*) or monkey (*dashed lines*) absorption parameters. Study A is described in reference (38); Studies B and C are described in reference (39).

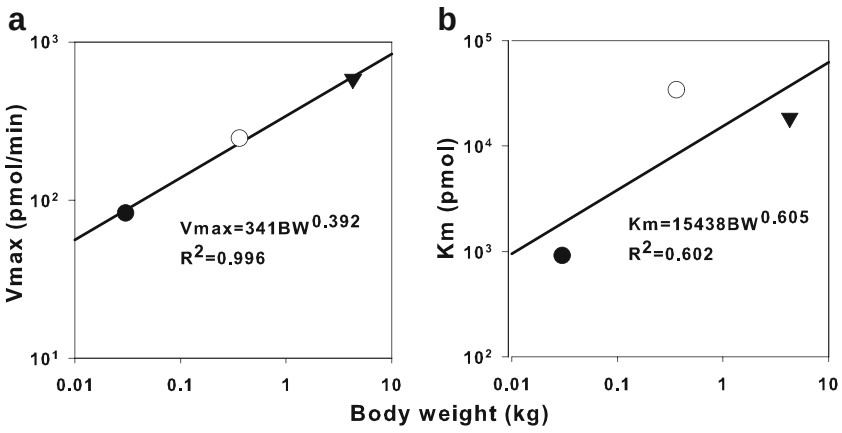

Fig. 5 Allometric relationships for absorption parameter estimates obtained from simultaneous fitting of mouse, rat, and monkey profiles: (**a**) Michaelis-Menten capacity (V_{max}) and (**b**) affinity (K_m) *versus* body weight. *Symbols* represent values from different species (mouse—●; rat—○; monkey—▼). *Lines* represent regression lines (Eq. 1).

useful for capturing observed data, it provides little insight into the mechanism of absorption and cannot be used effectively for interspecies scaling. Although the mechanism of exenatide absorption after SC injection is still unknown, absorptive transport appeared saturable. The Michaelis-Menten function well described the nonlinearity in exenatide absorption; however, one set of V_{max} and K_m was not able to capture pharmacokinetic profiles for all animals. Interestingly, a correlation was found between absorption parameters and species body weights (Fig. 5).

In projecting the pharmacokinetics of exenatide in humans, distribution and elimination parameters were successfully shared between animal and human models. The IV infusion profile in humans was successfully predicted using allometrically scaled V_c and k_{el} (allometric exponents were fixed to 1 and −0.25) and monkey values for R_{tot}^0 and k_{off}. Exenatide profiles following SC administration to humans could not be adequately predicted by utilizing monkey absorption parameters. On the other hand, rat V_{max} and K_m provided simulations, consistent with clinical data (Fig. 4). The second method, which utilized allometric expressions for V_{max} and K_m (allometric exponents were 0.392 and 0.605, see Fig. 5), also provided a good prediction of human pharmacokinetics. The large value of K_m (relative to dose) suggests that the ratio of V_{max} to K_m is most relevant for the apparent absorption rate. The ratio of V_{max} and K_m for humans is about 0.008 for Study B and 0.009 for Study C, which is very similar to 0.0125 reported from the analysis of exenatide human pharmacokinetics (22). This value is also similar to the ratio of V_{max} and K_m in rats (0.0072), which might explain why rat absorption parameters were best for simulating human SC profiles.

There are several limitations to this study. The data from several separate studies were combined, and any potential bias that might result from variability in experimental settings (including analytical assays) was disregarded. Individual animal data were not available, therefore the model was based on mean concentrations, and variability within each study could not be quantified. In addition, IV experiments with mice and monkeys contained relatively few data points and dose levels as compared to rat profiles, which might introduce bias into parameter estimates.

In summary, a TMDD model combined with allometric scaling was successfully used to simultaneously describe preclinical data for exenatide from three animal species following both IV and SC administration. The majority of model parameters could be shared among the animal species and further used for projecting exenatide behavior in humans. Receptor density and binding affinity estimated for monkeys can be used for predicting exenatide pharmacokinetics in humans following IV infusion. The absorption behavior in humans was best described using absorption parameters from rat (as compared to mouse or monkey) or using allometric scaling based on all three preclinical species. The modeling framework developed in this study can be potentially extended for interspecies scaling of the pharmacokinetics of other drugs that exhibit TMDD behavior.

ACKNOWLEDGMENTS AND DISCLOSURES

This research was supported, in part, by NIH grants GM57980 and HD071594. We thank Dr. John M. Harrold for his help in developing the MATLAB code for this project and Amylin Pharmaceuticals, Inc. for providing select preclinical and clinical datasets.

REFERENCES

1. Eng J, Kleinman WA, Singh L, Singh G, Raufman JP. Isolation and characterization of exendin-4, an exendin-3 analogue, from Heloderma suspectum venom. Further evidence for an exendin receptor on dispersed acini from guinea pig pancreas. J Biol Chem. 1992;267(11):7402–5.
2. Goke R, Fehmann HC, Linn T, Schmidt H, Krause M, Eng J, *et al.* Exendin-4 is a high potency agonist and truncated exendin-(9–39)-amide an antagonist at the glucagon-like peptide 1-(7–36)-amide receptor of insulin-secreting beta-cells. J Biol Chem. 1993;268(26):19650–5.
3. Gallwitz B, Ropeter T, Morys-Wortmann C, Mentlein R, Siegel EG, Schmidt WE. GLP-1-analogues resistant to degradation by dipeptidyl-peptidase IV *in vitro*. Regul Pept. 2000;86(1–3):103–11.
4. Parkes D, Jodka C, Smith P, Nayak S, Rinehart L, Gingerich R, *et al.* Pharmacokinetic actions of exendin-4 in the rat: comparison with glucagon-like peptide-1. Drug Dev Res. 2001;53(4):260–7.
5. Korner M, Stockli M, Waser B, Reubi JC. GLP-1 receptor expression in human tumors and human normal tissues: potential for *in vivo* targeting. J Nucl Med. 2007;48(5):736–43.
6. Parkes DG, Pittner R, Jodka C, Smith P, Young A. Insulinotropic actions of exendin-4 and glucagon-like peptide-1 *in vivo* and *in vitro*. Metabolism. 2001;50(5):583–9.
7. Arakawa M, Ebato C, Mita T, Hirose T, Kawamori R, Fujitani Y, *et al.* Effects of exendin-4 on glucose tolerance, insulin secretion, and beta-cell proliferation depend on treatment dose, treatment duration and meal contents. Biochem Biophys Res Commun. 2009;390(3):809–14.
8. Gedulin BR, Smith PA, Jodka CM, Chen K, Bhavsar S, Nielsen LL, *et al.* Pharmacokinetics and pharmacodynamics of exenatide following alternate routes of administration. Int J Pharm. 2008;356(1–2):231–8.
9. Ai G, Chen Z, Shan C, Che J, Hou Y, Cheng Y. Single- and multiple-dose pharmacokinetics of exendin-4 in rhesus monkeys. Int J Pharm. 2008;353(1–2):56–64.
10. Mager DE, Neuteboom B, Efthymiopoulos C, Munafo A, Jusko WJ. Receptor-mediated pharmacokinetics and pharmacodynamics of interferon-beta1a in monkeys. J Pharmacol Exp Ther. 2003;306(1):262–70.
11. Woo S, Jusko WJ. Interspecies comparisons of pharmacokinetics and pharmacodynamics of recombinant human erythropoietin. Drug Metab Dispos. 2007;35(9):1672–8.
12. Gao W, Jusko WJ. Pharmacokinetic and pharmacodynamic modeling of exendin-4 in type 2 diabetic Goto-Kakizaki rats. J Pharmacol Exp Ther. 2011;336(3):881–90.
13. Dedrick RL. Animal scale-up. J Pharmacokinet Biopharm. 1973;1(5):435–61.

14. Mahmood I, Balian JD. Interspecies scaling: predicting clearance of drugs in humans. Three different approaches. Xenobiotica. 1996;26(9):887–95.
15. Mahmood I. Application of fixed exponent 0.75 to the prediction of human drug clearance: an inaccurate and misleading concept. Drug Metabol Drug Interact. 2009;24(1):57–81.
16. McDonald TA, Zepeda ML, Tomlinson MJ, Bee WH, Ivens IA. Subcutaneous administration of biotherapeutics: current experience in animal models. Curr Opin Mol Ther. 2010;12(4):461–70.
17. Li L, Yang G, Li Q, Tan X, Liu H, Tang Y, *et al.* Exenatide prevents fat-induced insulin resistance and raises adiponectin expression and plasma levels. Diabetes Obes Metab. 2008;10 (10):921–30.
18. Mager DE, Jusko WJ. General pharmacokinetic model for drugs exhibiting target-mediated drug disposition. J Pharmacokinet Pharmacodyn. 2001;28(6):507–32.
19. Copley K, McCowen K, Hiles R, Nielsen LL, Young A, Parkes DG. Investigation of exenatide elimination and its *in vivo* and *in vitro* degradation. Curr Drug Metab. 2006;7(4):367–74.
20. Widmann C, Dolci W, Thorens B. Agonist-induced internalization and recycling of the glucagon-like peptide-1 receptor in transfected fibroblasts and in insulinomas. Biochem J. 1995;310(Pt 1):203–14.
21. Kagan L, Abraham AK, Harrold JM, Mager DE. Interspecies scaling of receptor-mediated pharmacokinetics and pharmacodynamics of type I interferons. Pharm Res. 2010;27(5):920–32.
22. Fineman M, Phillips L, Jaworowicz DJ, Cirincione B, Ludwig E, Taylor K, *et al.*, editors. Model-based evaluations to select and confirm doses in the clinical development of exenatide. American Society for Clinical Pharmacology and Therapeutics; 2007 March 21–24; Aneheim, CA.
23. Cosson VF, Fuseau E, Efthymiopoulos C, Bye A. Mixed effect modeling of sumatriptan pharmacokinetics during drug development. I: Interspecies allometric scaling. J Pharmacokinet Biopharm. 1997;25(2):149–67.
24. Martin-Jimenez T, Riviere JE. Mixed-effects modeling of the interspecies pharmacokinetic scaling of oxytetracycline. J Pharm Sci. 2002;91(2):331–41.
25. Mordenti J, Chen SA, Moore JA, Ferraiolo BL, Green JD. Interspecies scaling of clearance and volume of distribution data for five therapeutic proteins. Pharm Res. 1991;8(11):1351–9.
26. Gao W, Jusko WJ. Target-mediated pharmacokinetic and pharmacodynamic model of exendin-4 in rats, monkeys, and humans. Drug Metab Dispos. 2012;40(5):990–7.
27. Mager DE, Krzyzanski W. Quasi-equilibrium pharmacokinetic model for drugs exhibiting target-mediated drug disposition. Pharm Res. 2005;22(10):1589–96.
28. Goke R, Larsen PJ, Mikkelsen JD, Sheikh SP. Identification of specific binding sites for glucagon-like peptide-1 on the posterior lobe of the rat pituitary. Neuroendocrinology. 1995;62(2):130–4.
29. Satoh F, Beak SA, Small CJ, Falzon M, Ghatei MA, Bloom SR, *et al.* Characterization of human and rat glucagon-like peptide-1 receptors in the neurointermediate lobe: lack of coupling to either stimulation or inhibition of adenylyl cyclase. Endocrinology. 2000;141(4):1301–9.
30. Chicchi GG, Cascieri MA, Graziano MP, Calahan T, Tota MR. Fluorescein-Trp25-exendin-4, a biologically active fluorescent probe for the human GLP-1 receptor. Peptides. 1997;18(2):319–21.
31. Schepp W, Schmidtler J, Riedel T, Dehne K, Schusdziarra V, Holst JJ, *et al.* Exendin-4 and exendin-(9–39)NH2: agonist and antagonist, respectively, at the rat parietal cell receptor for glucagon-like peptide-1-(7–36)NH2. Eur J Pharmacol. 1994;269 (2):183–91.
32. Kagan L, Turner MR, Balu-Iyer SV, Mager DE. Subcutaneous absorption of monoclonal antibodies: role of dose, site of injection, and injection volume on rituximab pharmacokinetics in rats. Pharm Res. 2012;29(2):490–9.
33. Macdougall IC, Jones JM, Robinson MI, Miles JB, Coles GA, Williams JD. Subcutaneous erythropoietin therapy: comparison of three different sites of injection. Contrib Nephrol. 1991;88:152–6. discussion 7–8.
34. Sinha VK, Vaarties K, De Buck SS, Fenu LA, Nijsen M, Gilissen RA, *et al.* Towards a better prediction of peak concentration, volume of distribution and half-life after oral drug administration in man, using allometry. Clin Pharmacokinet. 2011;50(5):307–18.
35. Chiou WL, Barve A. Linear correlation of the fraction of oral dose absorbed of 64 drugs between humans and rats. Pharm Res. 1998;15(11):1792–5.
36. Zhao YH, Abraham MH, Le J, Hersey A, Luscombe CN, Beck G, *et al.* Evaluation of rat intestinal absorption data and correlation with human intestinal absorption. Eur J Med Chem. 2003;38 (3):233–43.
37. Jolling K, Perez Ruixo JJ, Hemeryck A, Vermeulen A, Greway T. Mixed-effects modelling of the interspecies pharmacokinetic scaling of pegylated human erythropoietin. Eur J Pharm Sci. 2005;24 (5):465–75.
38. Fehse F, Trautmann M, Holst JJ, Halseth AE, Nanayakkara N, Nielsen LL, *et al.* Exenatide augments first- and second-phase insulin secretion in response to intravenous glucose in subjects with type 2 diabetes. J Clin Endocrinol Metab. 2005;90(11):5991–7.
39. Kolterman OG, Kim DD, Shen L, Ruggles JA, Nielsen LL, Fineman MS, *et al.* Pharmacokinetics, pharmacodynamics, and safety of exenatide in patients with type 2 diabetes mellitus. Am J Health Syst Pharm. 2005;62(2):173–81.
40. Bjerre Knudsen L, Madsen LW, Andersen S, Almholt K, de Boer AS, Drucker DJ, *et al.* Glucagon-like Peptide-1 receptor agonists activate rodent thyroid C-cells causing calcitonin release and C-cell proliferation. Endocrinology. 2010;151(4):1473–86.